

# NUMERICAL INVESTIGATION ON THE FLOW CHARACTERISTICS OF A SUPERSONIC JET IMPINGING ON AN AXI-SYMMETRIC DEFLECTOR

S.Sankaran, M.Rajeswara Rao, T.N.V.Satyanarayana, N.Satyanarayana  
K.Visvanathan & Rupesh B. Kotapati\*

Scientist, Vehicle Assembly & Static Testing Division, SHAR Centre, ISRO  
Sriharikota - 524 124, INDIA

\*Research Assistant, Dept. of Mechanical & Aerospace Engineering  
Arizona State University, AZ 85287, USA

**Keywords :** Impinging supersonic jets, Axi-symmetric jet deflector, Shock pattern, Nozzle stand-off distance, Lift-off scenario

## Abstract

*The present study deals with the impingement characteristics of a supersonic jet issuing out of a convergent-divergent nozzle over an axi-symmetric jet deflector. An attempt has been made to numerically compute this impingement flow field during the rocket lift-off scenario. An axi-symmetric Navier-Stokes code has been used which adopts a control volume based finite difference scheme with  $k-\epsilon$  turbulence model. During the rocket lift-off scenario, the distance between the nozzle exit and the apex of the jet deflector ( $L/D_e$ ) varies gradually, where,  $L$  is the distance between the nozzle exit and the apex of the jet deflector at particular time ( $t$ ) and  $D_e$  is nozzle exit diameter. The numerical flow visualization obtained for each case indicates a change in the resulting flow field. The present study gives the quantitative and qualitative differences in the impingement flow field for some typical  $L/D_e$  cases during the rocket lift-off scenario.*

## 1 Introduction

Multiple supersonic jets find application in a variety of fields such as VTOL/STOL aircraft, sustainer rockets with strap-on boosters, gas burners, supersonic combustors, and noise reduction mechanisms for aero engines. The flow fields of the high speed jets exhibit many complex features such as the existence of shock

cells, sub-atmospheric reverse flow region between jets, entrainment of ambient fluid, jet bending and eventual merger etc. The characteristics of a supersonic jet are characterized by the stagnation pressure ratio ( $P_0/P_a$ ), exit Mach number ( $M_e$ ) and the nozzle configuration. The present study deals with the impingement characteristics of a supersonic jet issuing out of a convergent-divergent nozzle over an axi-symmetric jet deflector. An attempt has been made to numerically compute this impingement flow field during the rocket lift-off scenario.

An axi-symmetric Navier Stokes code has been used which adopts a control volume based finite difference scheme with  $k-\epsilon$  turbulence model to solve this complex flow problem. The resulting Mach number, pressure and temperature distributions along the centerline and also along the jet deflector wall are computed for the various cases of nozzle stand-off distance ( $L/D_e$ ) such as 3.0, 4.2, 6.3, 8.4, 12.6, 16.8 (Fig.1). The present study gives the quantitative and qualitative differences in the impingement flow field for all  $L/D_e$  cases. The present Navier Stokes code solved for axi-symmetric cases shows a good agreement with the experimental results carried out by Prasad et al (1993). This exercise was done to validate the finite difference scheme adopted for this investigation.

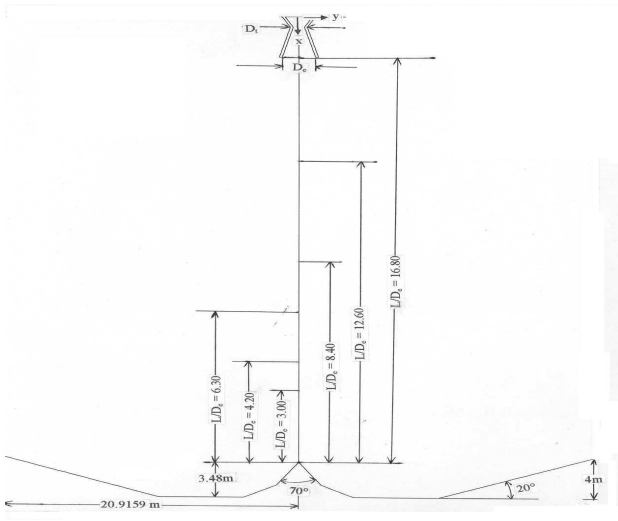


Fig.1 General configuration employed

## 2 Brief Literature Review

Many experiments have been carried out to study free jets [1-6]. A comprehensive experimental investigation of supersonic free jets was reported by Love et al [4]. Abdel-Fattah has measured shock cell lengths for supersonic jets coming out of convergent-divergent nozzles in conjunction with schlieren pictures [2]. Solution of parabolic Navier-Stokes equations using the shock capturing method for the single and two-phase supersonic region was presented by Dash and Wolf [7]. The solution of unsteady Euler equations to obtain the flow field of underexpanded two-dimensional free jets was carried out by Sinha et al using the finite difference scheme [8]. Dash et al have made extensive numerical investigations on the underexpanded jets [9]. These studies on free jets reveal that the time-marching method can capture the flow field features. The impingement flow field produced due to the impingement of underexpanded supersonic jets on inclined and perpendicular flat plates have been extensively studied by Lamont & Hunt [3]. The shadow graph and surface pressure distribution on a conical geometry due to impingement of axi-symmetric jets were investigated by Jennions and Hunt [10]. Most of these experiments were performed to study free

jets or impinging jets on solid obstacles such as, flat plates, cones and wedges.

In the present paper, computations were carried out to investigate impingement flow field on a typical axi-symmetric jet deflector. An attempt has been made to numerically simulate the impinging flow field during the rocket lift off scenario. The present study has brought out the effect of  $L/D_e$  on the flow characteristics through numerical flow visualization obtained from these studies.

## 3 Description of Mathematical Model

The two-dimensional, compressible flow has been solved using Reynolds averaged Navier-Stokes equation with k-ε turbulence model. The governing equations for the flow problem can be expressed as,

$$\frac{\partial Q}{\partial t} + \frac{\partial E}{\partial z} + \frac{\partial F}{\partial r} + \alpha H = \frac{\partial J_z}{\partial z} + \frac{\partial J_r}{\partial r}$$

where, 
$$Q = \begin{Bmatrix} \rho \\ \rho u \\ \rho v \\ \rho e \end{Bmatrix};$$

$$E = \begin{Bmatrix} \rho u \\ \rho u^2 + p \\ \rho uv \\ \rho u (e + p/\rho) \end{Bmatrix}; \quad F = \begin{Bmatrix} \rho v \\ \rho uv \\ \rho v^2 + p \\ \rho v (e + p/\rho) \end{Bmatrix}$$

Also, the vector H represents the curvature forms in cylindrical co-ordinates and  $J_z$  and  $J_r$  denote viscous stress terms. The viscous stresses are evaluated using the equivalent viscosity,

$$\mu = \mu_l + \mu_t.$$

The turbulent viscosity,  $\mu_t$  is evaluated with the help of the k-ε model using compressibility correction. The temperature, pressure and density are related through the state equation,

$$p = \rho RT$$

All these equations have been solved using a control volume based finite difference scheme for various chamber pressure values. In the  $k - \epsilon$  turbulence model, these scales are obtained from two parameters,  $k$  (turbulent kinetic energy) and  $\epsilon$  (dissipation rate of kinetic energy). The velocity and length scales are taken as  $\sqrt{k}$  and  $\sqrt{k^3/\epsilon}$  respectively.

### 3.1 Turbulence Model

For high-speed jet flows, the problem is further complicated due to compressibility effect. In the near field, the flow is essentially inviscid, while further downstream, it becomes turbulent and it intensely mixes with ambient fluid. In the present study, the two-equation  $k-\epsilon$  turbulence model (Launder and Spalding, 1974) that is based on the generalized Boussinesq eddy viscosity concept (Hinze, 1975) is employed. This model employs two partial differential equations to estimate the velocity and length scales and hence it is known as a two-equation model. The Reynolds stresses are given by:

$$-\overline{\rho u_i u_j} = \mu_t \left( \frac{\partial U_i}{\partial x_j} + \frac{\partial U_j}{\partial x_i} \right) - \frac{2}{3} \delta_{ij} \rho k$$

where  $\delta_{ij}$  is the Kronecker-delta function,  $u_i$  represents the turbulent velocity fluctuations and  $\mu_t$  is the turbulent viscosity that is related to the kinetic energy of turbulence ( $k$ ) and its dissipation rate ( $\epsilon$ ) by dimensional analysis. Thus,

$$\mu_t = C_\mu \rho k^2 / \epsilon$$

where  $C_\mu = 0.09$  [Launder and Spalding, (1974)]. The two differential equations, which govern the transport of turbulent kinetic energy,  $k$  and its dissipation rate  $\epsilon$  are given by,

$$\frac{\partial}{\partial x_j} (\rho U_j k) = \frac{\partial}{\partial x_j} \left[ \left( (\mu_t + \mu) / \sigma_k \right) \frac{\partial k}{\partial x_j} \right] - \rho u_i u_j \frac{\partial U_i}{\partial x_j} - \rho \epsilon$$

$$\frac{\partial}{\partial x_j} (\rho U_j \epsilon) = \frac{\partial}{\partial x_j} \left[ \left( (\mu_t + \mu) / \sigma_\epsilon \right) \frac{\partial \epsilon}{\partial x_j} \right] - C_1 \frac{\epsilon}{k} \rho u_i u_j \frac{\partial U_i}{\partial x_j} - C_2 \rho \epsilon^2 / k$$

where,  $C_1$  and  $C_2$  are further constants in this model with values  $C_1=1.44$  and  $C_2 = 1.92$ . Moreover, the turbulent Prandtl numbers for  $k$  and  $\epsilon$  are given by  $\sigma_k = 1.0$  and  $\sigma_\epsilon = 1.3$ , respectively. The above equations could be modified after substitution and the resulting system of six coupled equations for six unknowns completes the closure problem for the turbulent flow investigated.

### 3.2 Boundary Conditions Employed

To complete the physical problem specification, boundary conditions are supplied at each boundary segment of the flow domain (Fig.2). The boundary conditions employed for the simulation of the supersonic jet flow in the present study are,

**Inflow** : The inlet conditions for supersonic flows are specified in terms of the total pressure and total temperature,  $P_o$  and  $T_o$  respectively.

$$P_{in} = P_o ; T_{in} = T_o$$

**Far stream boundary** : The jet flow becomes subsonic at a large distance; hence, the pressure at far stream is prescribed as atmospheric value and other parameters are smoothly extrapolated.

$$\frac{\partial^2 u}{\partial x^2} = \frac{\partial^2 v}{\partial x^2} = \frac{\partial^2 w}{\partial x^2} = 0 ;$$

$$p = p_{atm}$$

**Wall boundary**: At wall boundaries, no-slip condition is prescribed and walls are taken as adiabatic.

$$u = v = w = 0, \frac{\partial T}{\partial n} = 0 ;$$

**Symmetric boundary** : A zero normal gradient is applied for the variables  $u$ ,  $p$  and  $T$  at the symmetry boundaries. Also the normal velocity components vanish at symmetric boundary.

$$\frac{\partial u}{\partial y} = \frac{\partial p}{\partial y} = \frac{\partial T}{\partial y} = 0 ; v = w = 0$$

In turbulent flows, the turbulent intensity and characteristic length are also specified to calculate the  $k$  and  $\epsilon$  at the inlet boundary and

diffusion of all scalars at the inlet is assumed to be zero. The boundary conditions for  $k$  and  $\epsilon$  at the far-stream and symmetry boundaries are similar to those of temperature. Near the walls, the wall function approach is employed (Launder and Spalding (1974)).

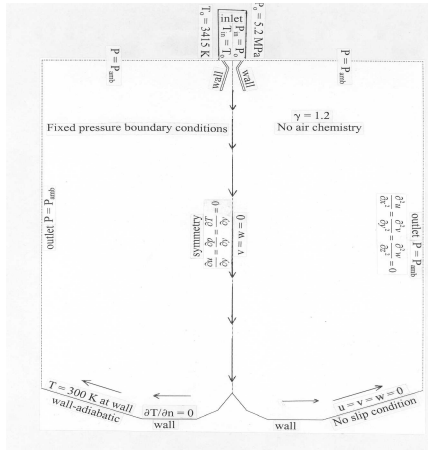


**Fig.2 Boundary conditions employed**

### 3.3 Grid used

The full geometry as shown in Fig. 1 earlier has been considered for simulation. The configuration has a convergent-divergent nozzle along with an axi-symmetric jet deflector. As the configuration under study is a classical axi-symmetric case, one half of the geometry is only considered for discretisation and solving (Fig.3). This is done particularly to minimize the CPU time. During post-processing, the results have been symmetrically copied to generate data corresponding to the whole geometry, for the sake of understanding. The partial differential equations and boundary conditions of the problem are converted into a set of non-linear algebraic equations by integrating each of the governing equations over the control volumes formed by the grid system. The solutions for the resulting algebraic system are obtained using suitable iterative solvers.

#### 3.3.1 Grid Independency Test

A non-staggered structural grid of size 200x150 using a body fitted coordinate system has been

adopted for the present study. This present grid size has been arrived based on the grid independency test. Various grid sizes such as 100x50, 140x100, 160x98, 125x100, and 200x150 have been tried and the distribution of the centerline Mach number has been plotted for all cases. From this result, it has been found that the grid size of 200 X 150 is optimal in view of the lower CPU time, solution accuracy, and faster convergence. Figure 3 shows the geometry and corresponding grid used for computation purpose.

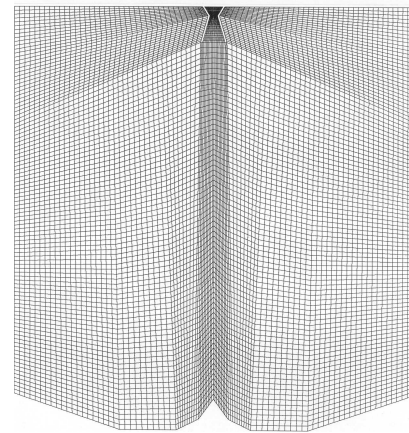


**Fig.3 Grid employed (200 X 150)**

#### 3.3.2 Convergence Criteria

Final convergence is decided by way of the residual-source criterion, which measures the deviation from exactness for all flow variables. The convergence criteria for the present study has been set as the sum of normalized residual value (including the variables of mass,  $u$ ,  $v$ ,  $H$ ,  $k$  and  $\epsilon$  being equal to  $1 \times 10^{-3}$ ). The computations were under relaxed to provide stability to the iterative procedure. The under relaxation factors are 0.7 for  $u$ ,  $v$ , 0.5 for pressure and 0.8 for temperature.

### 4 Results and Discussion

Attempts were made to numerically visualise the flow pattern of a supersonic jet issuing out of a convergent divergent nozzle and impinging over an axi-symmetric jet deflector, for various cases of nozzle stand-off distances ( $L/De$ ) viz.,

## NUMERICAL INVESTIGATION ON THE FLOW CHARACTERISTICS OF A SUPERSONIC JET IMPINGING ON AN AX-SYMMETRIC DEFLECTOR

3.0, 4.20, 6.30, 8.40, 12.60 and 16.80. The present code could capture the complex flow pattern along with shocks for various cases mentioned above.

### 4.1 Variation of Mach number

Figures 4a to f give the Mach number contours for all the cases ( $L/D_e = 3.00, 4.20, 6.30, 8.40, 12.60$  and  $16.80$ ). The Mach number contours depict the structure of the flow including the shock pattern for all cases. It is evident from the figures that the strength of the shock near the apex of the jet deflector decreases enormously as the magnitude of the  $L/D_e$  increases. Especially for the cases of  $L/D_e = 12.60$  and  $16.80$ , the flow has become nearly subsonic near the leading edge of the deflector. To bring out these differences, the variation of the centerline Mach number is plotted for all cases in Fig.5. Here, the distance between the nozzle exit and the apex of the jet deflector ( $L$ ) is used to non-dimensionalise any distance ( $x$ ) along the centerline. For the case of  $L/D_e = 3.00$ , it is seen that the second shock cell sits prettily on the apex of the jet deflector. With the increase of  $L/D_e$ , the Mach number along the centerline varies significantly (decreases in the axial direction). The effect of supersonic flow is found to be nearly absent for the last two cases ( $L/D_e = 12.60, 16.80$ ).

To have a better insight of the flow field, the Mach number distribution along the jet deflector wall for all cases are plotted together in Fig. 6 to represent the effect of Mach number pictorially in the whole computational domain. From figure, it is seen that the shock-shear layer interaction takes place predominantly within the initial 30% of the jet deflector length along the radial direction. Beyond  $y/r = 10$ , the Mach number seems to be nearly constant for all the cases of  $L/D_e$ . However, for the cases of  $L/D_e = 12.60$  and  $16.80$ , the variation is found to be entirely different from other cases. It is quite interesting to note that the Mach number value at the apex of the deflector for  $L/D_e = 3.00$  is less than that for  $L/D_e = 4.20$ . For the critical

case of  $L/D_e = 3.00$ , the value of Mach number is found to be slightly lower than the subsequent case of  $L/D_e = 4.20$ , beyond which there is a definite decay in the maximum Mach number value with the increase in  $L/D_e$ .

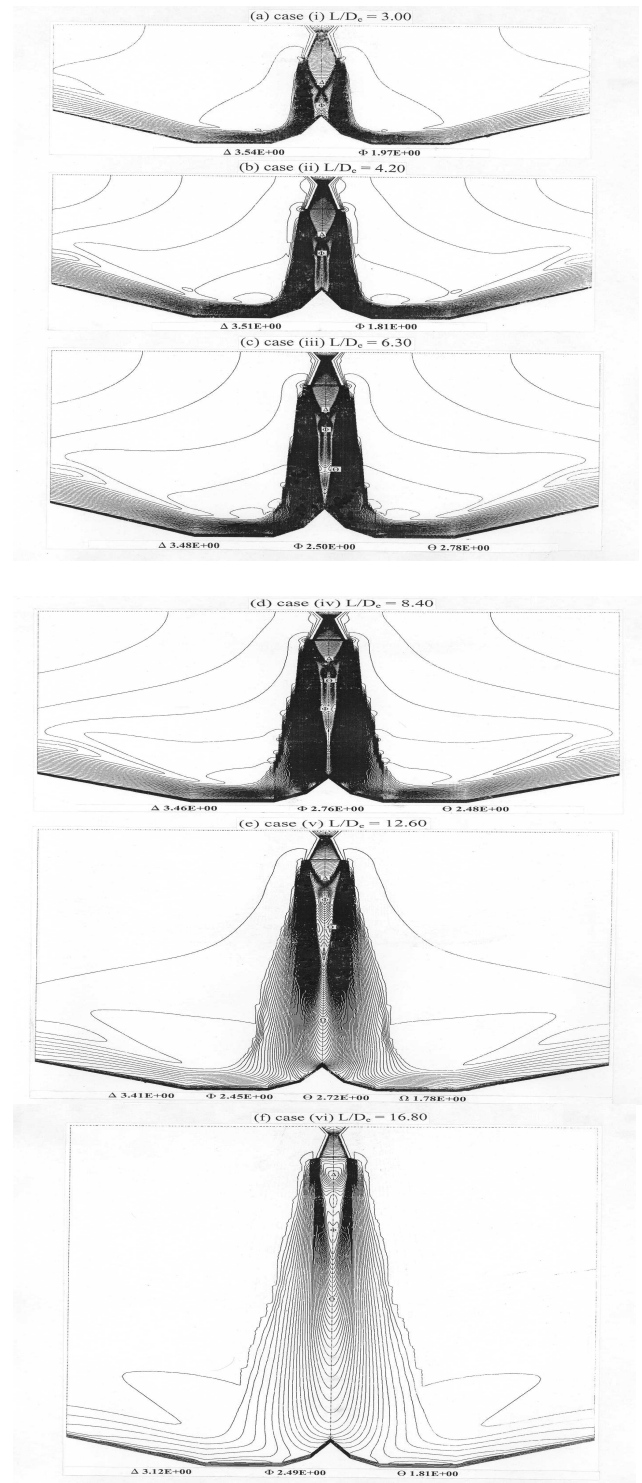


**Fig.4 Mach contours for various  $L/D_e$  cases**

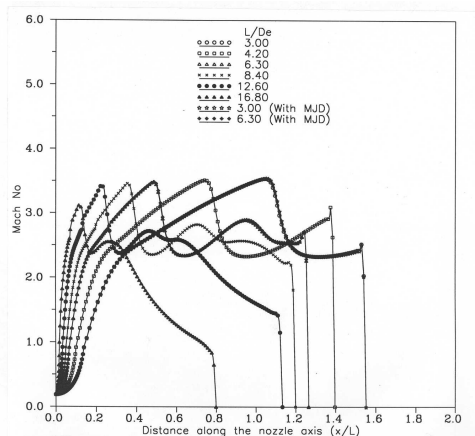


Fig.5 Variation of centerline Mach number

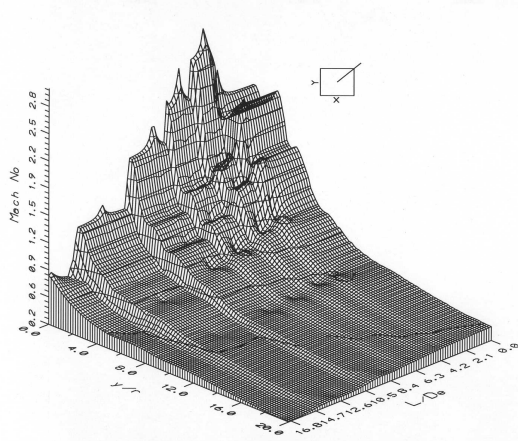


Fig.6 Overall variation of Mach number along the deflector wall

#### 4.2 Static pressure distribution

The static pressure distribution obtained computationally along the jet deflector wall for all cases is presented in Fig.7. The severe pressure variation near the apex of the jet deflector, in particular for the cases  $L/D_e = 3.00$ ,  $4.20$ ,  $6.30$  and  $8.40$  shows a weak reflected shock pattern existing in that region. However, such variations are not found in a predominant manner for the later two cases of  $L/D_e = 12.60$  and  $16.80$ . For all cases, the static pressure has become nearly equal to that of the ambient value at around  $y/r = 11$ , that is, within the 50% of the jet deflector length where, the interaction

between the shock and the viscous shear layer seems to be over.

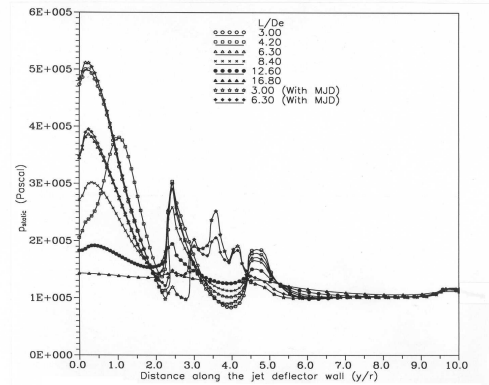


Fig. 7 Variation of pressure along the deflector wall

Beyond this location, the variation in the static pressure is absent for all the cases considered. It is evident that the level of interaction is very high for lower  $L/D_e$  cases when compared to that of higher  $L/D_e$  cases. It is obvious that when the distance between the nozzle exit and the apex of the deflector is small, the interactions are very severe within the initial 30% of the jet deflector length. Moreover, the structure of the flow is expected to be different for different  $L/D_e$  cases, which is seen from the static pressure distribution plots.

The centerline static pressure variation (along the nozzle axis) is plotted for all cases in Fig.8.

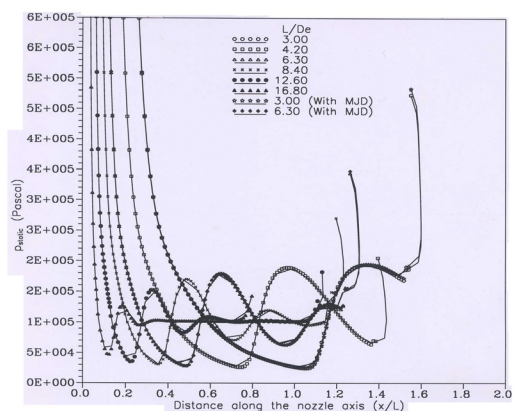


Fig. 8 Centerline static pressure variation

From the above figure, it is evident that for all cases considered, the pressure near the apex of the deflector is higher when compared to any

## NUMERICAL INVESTIGATION ON THE FLOW CHARACTERISTICS OF A SUPERSONIC JET IMPINGING ON AN AX-SYMMETRIC DEFLECTOR

other location along the centerline. Moreover, the oscillations in the pressure in the region of  $x/L = 0.2$  to  $1.6$  indicate the existence of a multiple shock pattern and the resulting interaction of shock and shear layer with the ambient fluid. In the last two cases ( $L/D_e = 12.60$  and  $16.80$ ), it is seen that the variations are not that much predominant, in the region  $x/L = 0.2$  to  $1.1$ .

The magnitude of pressure at the apex of the jet deflector ( $y/r = 0$ ) for all  $L/D_e$  cases is presented in Fig. 9.

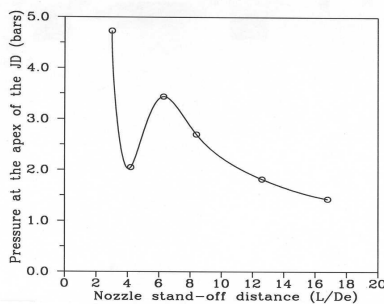


**Fig.9 Distribution of pressure at the apex of the deflector**

From this, it can be deduced that the value of static pressure generally decreases as  $L/D_e$  increases, except for the case  $L/D_e = 4.20$ . It is quite interesting to note that the value of the static pressure for the case  $L/D_e = 4.20$  is much less than that for the later two cases of  $L/D_e = 6.30$  and  $8.40$ . The reason for the sudden drop in pressure for the case  $L/D_e = 4.20$  can only be attributed to the specific characteristics of a supersonic jet impinging on an axi-symmetric deflector.

To understand the flow behaviour along the jet deflector wall, the locations of the maximum pressure value are plotted for all  $L/D_e$  cases in Fig.10. It is seen here that the location of the maximum pressure lies just away from the apex of the jet deflector ( $y/r = 1$ ) rather than exactly on the apex as for the other two cases ( $L/D_e = 3.00$  and  $6.30$ ;  $y/r = 0$ ). However, this variation is found to be minor considering the overall length of the deflector. It can be said that for all cases, the maximum pressure lies within the

initial 5% of deflector length. The surfer plot presented in Fig.11 gives the overall variation of static pressure along the deflector wall for all cases, and shows a definite uniform trend within them barring certain non-uniformities at certain locations.

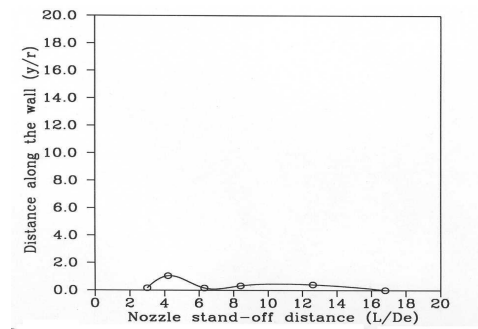


**Fig.10 Location of maximum pressure along the deflector wall**

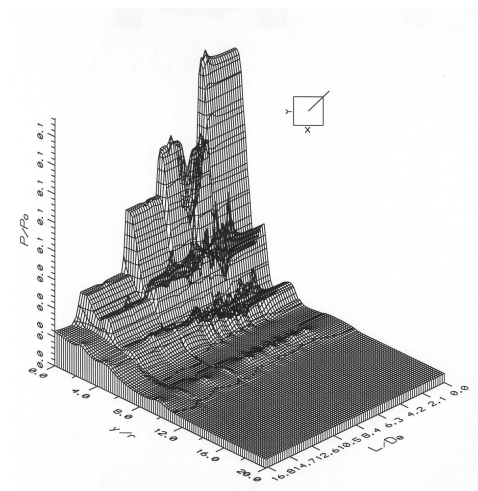


**Fig.11 Overall variation of pressure along the deflector wall**

### 4.3 Validation for the present study

The present code was validated by comparing the flow fields obtained by Prasad *et al* (1995) experimentally [6]. Prasad *et al* (1995) have carried out an experimental investigation of the impingement flow field produced by an under expanding supersonic jet on a typical axi-symmetric jet deflector. The experiments consist of Schlieren flow visualization and

measurements of pressure during the lift-off phase of a rocket. They have used a convergent-divergent nozzle, which produces a jet exit Mach number of 2.2 with expansion ratio of 1.2. The experiments have been carried out using a wind tunnel with air as the working fluid with a ambient temperature of 300K ( $\gamma = 1.4$ ). Two different nozzle stand-off distances ( $L/D_e = 2.0$  and 3.0) have been tested using this facility and are reported in the literature.

The above said geometry was simulated using the present code and the flow fields were computed for  $\gamma = 1.4$  using air as the driving fluid. Figures 12a and b give the static pressure distributions along the jet deflector wall for the two cases,  $L/D_e = 2.0$  and 3.0. It is seen that there exists a good match between the experimental results and the computational results for both  $L/D_e = 2.0$  and 3.0.

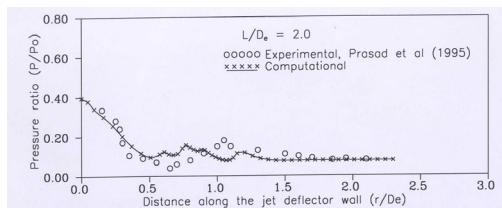


**Fig.12a Variation of pressure along the wall ( $L/D_e = 2.0$ )**

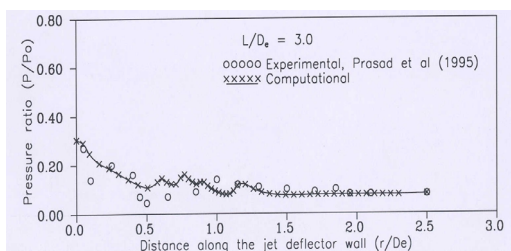


**Fig.12b Variation of pressure along the wall ( $L/D_e = 3.0$ )**

Experimentally obtained Schlieren images for the above cases ( $L/D_e = 2.0$  and 3.0) reported by Prasad et al (1995) are presented in Figs. 13a and b to 15a and b for comparison purpose. From the above results, it is seen that there is a good match between the Schlieren pictures and the numerical visualization pictures obtained from the present study.

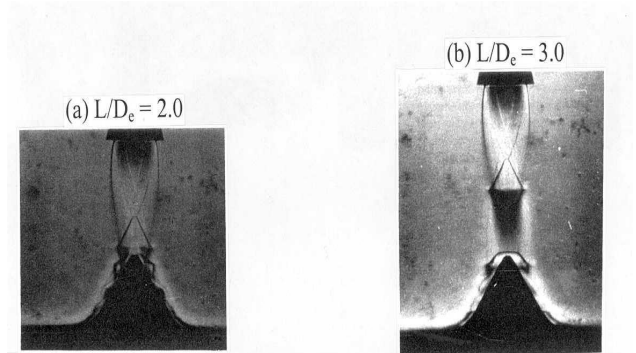


**Fig.13 Schlieren images for the validation cases**

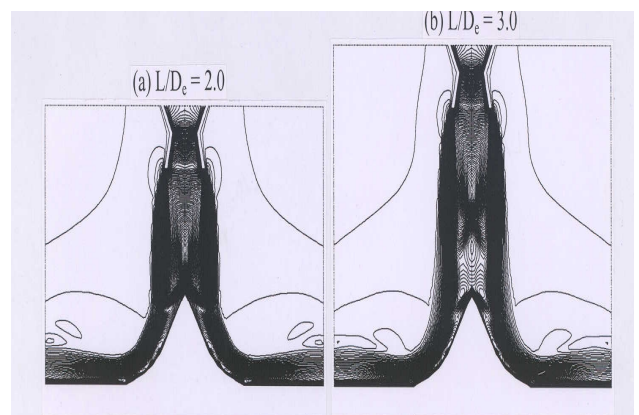


**Fig.14 Computationally obtained Mach contours for the validation cases**

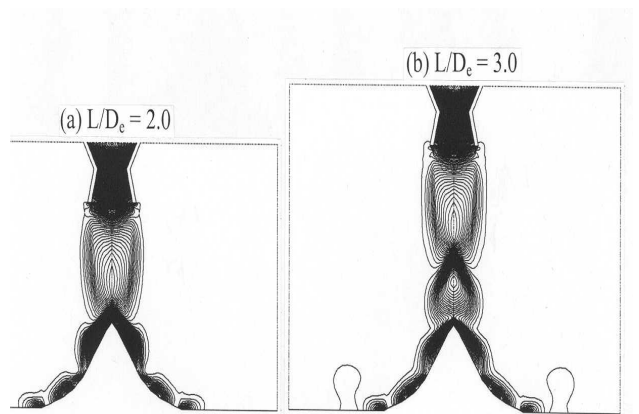


**Fig.15 Computationally obtained pressure contours for the validation cases**

## 5 Concluding Remarks

The present investigation could bring out the impinging flow fields on and around the jet deflector including the complex shock structures. Both quantitatively and qualitatively,

## NUMERICAL INVESTIGATION ON THE FLOW CHARACTERISTICS OF A SUPERSONIC JET IMPINGING ON AN AX-SYMMETRIC DEFLECTOR

better comparisons were obtained between the computational and experimental results available in the literature. The present study would be very useful during the preliminary design of the jet deflector. The differences in the flow field for the various cases of  $L/D_e$  would also help to arrive at an exact configuration of the jet deflector for launching advanced propulsion systems.

### References

1. **Seiner, J.M., Manning J.C., and Ponton,M.K.** Dynamic pressure loads associated with twin supersonic plume resonance. *AIAA Journal*, **26**, 954-960,1988.
2. **Abel-Fattah, A.M.** Discrete Tone emission from high pressure ratio supersonic jets from convergent divergent nozzle. *AIAA Journal*, **26**, 283-291, 1988.
3. **Lamont, P. H. and Hunt, B.L.** The impingement of the under-expanded axisymmetric jets on wedges. *Journal of Fluid Mechanics*, **76**, part 2, 307-336,1976.
4. **Love, E.S.** An approximation of the boundary of a supersonic axisymmetric jet exhausting into a supersonic stream. *Journal of the Aeronautical Sciences*, February, 130-131,1958.
5. **Patankar, S.V.** *Numerical Heat Transfer and Fluid Flow*. Hemisphere Publishers, Washington DC, 1980.
6. **Prasad, J.K., Mehta,R.C. and Srikanth,A.K.** Impingement of supersonic jets on an axisymmetric deflector. *AIAA Journal*, **32**, 1535-1538,1994.
7. **Dash, S.M., and Wolf, D.F.** Fully coupled analysis of jet mixing problem, Part-I, Shock capturing model, SCIPVIS, NASA – CR-3761,1984.
8. **Sinha,R., Zakky, V. and Erdos, J.** Flow field analysis of plumes of two-dimensional under-expanded jets by a time dependent method. *AIAA Journal*, **9(12)**,2363-2370, 1970.
9. **Dash,S.M., Pearce,B.E. and Pergament** Prediction of rocket plumes flow fields for IR signatures studies. *J. Spacecrafts and Rockets*, **17(3)**, 190-199, 1980.
10. **Jennions,I.K. and Hunt,B.L** The axisymmetric impingement of supersonic air jets on cones, *Aeronautics Quarterly*, **31**, 26-41,1980.